Applied Surface Science 626 (2023) 157253

Contents lists available at ScienceDirect

Applied Surface Science

journal homepage: www.elsevier.com/locate/apsusc

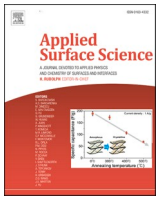

Full Length Article

# Atomistic insights into bias-induced oxidation on passivated silicon surface through ReaxFF MD simulation

Jian Gao, Xichun Luo *, Wenkun Xie, Yi Qin, Rashed Md. Murad Hasan, Pengfei Fan

*Centre for Precision Manufacturing, DMEM, University of Strathclyde, Glasgow G1 1XJ, UK*

ARTICLE INFO

*Keywords:*
Nanolithography
ReaxFF MD
Bias-induced oxidation
Chemical composition
Silicon

ABSTRACT

The study investigated the bias-induced oxidation through ReaxFF molecular dynamics simulations in order to bridge the knowledge gaps in the understanding of physical–chemical reaction at the atomic scale. Such an understanding is critical to realise accurate process control of bias-induced local anodic oxidation nanolithography. In this work, we simulated bias-induced oxidation by applying electric fields to passivated silicon surfaces and performed a detailed analysis of the simulation results to identify the primary chemical components involved in the reaction and their respective roles. In contrast to surface passivation, bias-induced oxidation led mainly to the creation of Si–O–Si bonds in the oxide film, along with the consumption of $H_2O$ and the generation of $H_3O^+$ in the water layer, whereas the chemical composition on the oxidised surface remained essentially unchanged with a mixture of Si–O–H, Si–H, Si–$H_2$, $H_2O$–Si and Si–O–Si bonds. Furthermore, parametric studies indicated that increased electric field strength and humidity did not significantly alter the surface chemical composition but notably enhanced the bias-induced oxidation, as indicated by the increased number of Si–O–Si bonds and oxide thickness in simulation results. A good agreement is achieved between the simulation and experimental results.

## 1. Introduction

Nanolithography through bias-induced local anodic oxidation (LAO) is one of the promising nanopatterning approaches that enable high-precision, direct and flexible fabrication of next-generation nano/quantum devices [1]. This technique uses sharp probes or nanostructured electrodes to induce controlled oxidation of a conductive surface, enabling the creation of localised oxide structures within a nanoscale region. Through precise control over oxidation growth, a wide range of nanostructures can be created, including nanodots/nanoholes, nanowires, and 3D nanostructures, that have proven to be useful in a variety of applications, including quantum dots [2], nanoelectronics [3] and optics [4]. Compared to optical lithography, electron or ion beam lithography, and nanoimprint lithography, LAO is a straightforward nanopatterning process with lower environmental requirements and implementation costs, making it an attractive option for nanopatterning on a simple platform. Recent advances with the use of multi-tip arrays or structured nanoelectrodes have demonstrated that LAO can enable large-scale nanopatterning on various materials [1,5].

An in-depth understanding of the underlying mechanism of physical and chemical reactions is very important to gain accurate process control in LAO with high-precision or even atomic or close-to-atomic scale precision [6]. Theogene et al [7] used finite element simulations to study the underlying mechanism of electric field enhancement in LAO process and decoupled the influence of applied voltage, tip curvature radius, semi-angle and tip-sample distance on electric field distribution. The research outcome indicated that high electric field enhancement can be achieved through a sharp tip with a small tip radius and a small semi-angle. Cramer et al [8] applied SPC/E potentials-based molecular dynamics (MD) simulations to reveal and visualise the microscopic details of the bias-induced build-up process of water bridge, which provided the molecular description of the threshold voltage and hysteresis behaviour. Choi et al [9] used the TIP3P model to simulate the water bridge formation, thinning and snap-off, and obtained the simulation results-based force-distance curve, which is well consistent with the experimental results. However, these simulation studies have not fully explained the underlying mechanism of chemical reaction between conductive substrate and water layer, which has become an important knowledge gap in further improving the manufacturing capability of LAO.

* Corresponding author.
*E-mail address:* xichun.luo@strath.ac.uk (X. Luo).

https://doi.org/10.1016/j.apsusc.2023.157253
Received 27 February 2023; Received in revised form 31 March 2023; Accepted 10 April 2023
Available online 15 April 2023

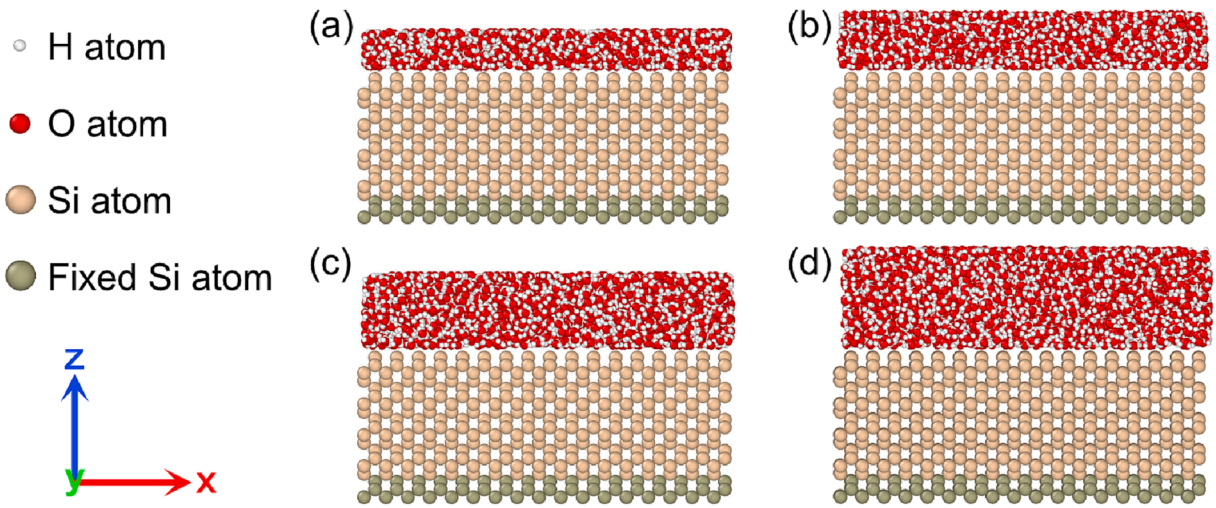


**Fig. 1.** Schematic views of silicon-water simulation models with water layer thicknesses of (a) 7, (b) 10, (c) 13 and (d) 17 Å.

Reactive force field (ReaxFF) MD simulation is an ideal method for handling chemical reactions within a large number of molecules. It not only offers irreplaceable advantages in elucidating bonding interaction, chemical composition and atomic dynamics behaviours, but also saves the computational cost when using first-principles methods [6,10,11]. This method has been successfully applied in the studies of surface oxidation [12–20], chemical mechanical polishing [21–26], nanoscale contact and tribology [27–29]. In the study of nanoelectrode lithography, Hasan et al [30,31] used ReaxFF MD simulation to investigate the bias-induced oxidation mechanism and its dependence on electric field, humidity, and crystallographic orientation. However, these studies assumed the oxidation began on a pristine silicon surface. In reality, upon the exposure to atmospheric humidity, a surface passivation layer was immediately formed on the surface before the introduction of electric field. It can be inferred that the existence of surface passivation layer will affect the subsequent bias-induced oxidation process, but it remains unclear. Therefore, the influence of the passivation layer on bias-induced oxidation is currently a significant knowledge gap in the literature, which requires an in-depth understanding of the physical–chemical reaction mechanisms of LAO at the atomics scale.

In order to address above-mentioned knowledge gaps, in this work, the water passivation and subsequent bias-induced oxidation processes of silicon (1 0 0) surface are investigated sequentially through ReaxFF MD simulations. Firstly, the spontaneous reaction process between silicon surfaces and water molecules is simulated without the application of electric field, thereby forming the passivation oxide on the silicon surface. Further, an electric field is introduced to simulate the subsequent bias-induced oxidation on the passivated silicon substrate. Based on the simulation results, the surface passivation and bias-induced oxidation are deeply investigated through a comprehensive analysis of bonds/particles number, atomic charge, and their evolution and distribution. In addition, the dependence of electric field and water layer thickness is studied, aiming to reveal the parametric effect on bias-induced oxidation process and the influencing mechanism.

## 2. Methodology

In this work, all simulations were conducted in LAMMPS [32] using the ReaxFF force field developed by Wen et al [21]. This force field has been extensively validated in previous studies on water–silicon interactions, chemical mechanical polishing of silicon and tribochemical wear at $Si/SiO_2$ interface in aqueous environment [12,21,33]. The charge equilibration (QEq) model was used to equilibrate the charge of simulation model at each time step [34]. To consider the influence of external electrical field in the simulations, standard LAMMPS code was modified through adding Coulomb energy in the ReaxFF potential [16]. Numerous studies on LAO have reported that connecting an external power supply to the nanoscale probe and substrate in close proximity can generate an enhanced electric field ranging from 1 to 10 V/nm [35,36]. In this work, we applied electric fields within this range to examine their effects on oxidation. The initial silicon-water model was constructed with a silicon (1 0 0) substrate with a size of 63.8305 × 63.8305 × 23.895 Å and a water layer which has a density of 1 g/cm$^3$ and consists of randomly distributed $H_2O$ molecules. Asay and Kim [37] investigated the surface adsorption of water and established a correlation between the thickness of water layers and relative humidity, as depicted in Fig. 2 of their study. Specifically, water layer thicknesses at 7, 10, 13, and 17 Å correspond to relative humidity levels of approximately 20%, 40%, 70%, and 90%, respectively. Based on this relationship, initial models with varying water layer thicknesses were constructed as shown in Fig. 1 to qualitatively express reaction models at different humidity levels. The lattice constant of silicon was set at 5.31 Å, which was proven to produce minimum energy in convergence simulation tests. The configuration of randomly distributed water molecules was built using PACKMOL [38]. To facilitate the simulation, periodic boundary conditions were applied to $x$ and $y$ directions and a shrink-wrapped boundary condition was applied to $z$ direction. To prevent atom lost, a reflecting wall was introduced on the top of water layer. The bottom silicon layer was fixed to prevent the overall movement. The temperature was set at 300 K, controlled by NVT ensemble with a damping constant of 10 fs. A timestep of 0.1 fs was used to achieve charge and bond order balance during the simulation [39,40]. Verlet algorithm has been adopted to integrate the atom trajectories. The particle/bond type and number, atomic charge and their distributions were counted and analysed using self-developed python programs. The visualisation of simulation results was assisted with OVITO [41].

## 3. Bias-induced oxidation on passivated Si (1 0 0) surface

Due to the existence of boundary dangling bonds, pure silicon surface has a high reactivity, and therefore a passivation layer is formed as soon as it contacts with water. The simulation of bias-induced oxidation in this work consists of two steps to simulate experimental conditions. The first step is to create the passivation layer by allowing a natural reaction between silicon and water, while the second step simulates further bias-induced oxidation by applying an electric field. The first ReaxFF MD simulation was performed for the model in Fig. 1 (b) for 2000 ps, during which no electric field was applied during initial 1000 ps, and then an electric field of 3.5 V/nm was applied from 1000 to 2000 ps.

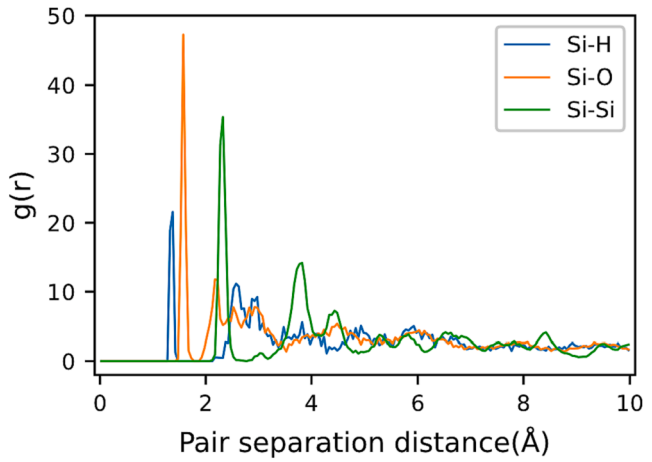


**Fig. 2.** RDF curves for Si–H, Si–O and Si–Si in oxide film formed by surface passivation.

### 3.1. Surface passivation

The MD simulation result at 1000 ps is shown in Fig. 3 (a). We can see that a number of O and H atoms were adsorbed on the silicon surface, and some O atoms penetrated the silicon substrate, thus forming a passivated oxide layer. In this work, we define the oxide film as the region between bottom oxygen atom and the top silicon atom along the *z* direction. To reveal the chemical composition and structure of the passivation layer, the partial radial distribution function (RDF) of oxide film is plotted and shown in Fig. 2. The peak of Si–H bond length is located at about 1.37 Å, which is close to the value of 1.48 Å reported in Ref [42]. Si–Si bonds have a peak length at 2.35 Å and Si–O bonds shows two peak lengths at 1.58 and 2.25 Å, which agree with the experimental values well [43–46]. After that, several peaks of Si–O appear between 3 and 7 Å, indicating amorphous structures within the oxide film.

A combined analysis of simulation results in Fig. 3 (a) and their RDF in Fig. 2 show that new bonds and particles including Si–O–H, Si–H, Si–$H_2$, $H_2O$–Si, Si–O–Si (siloxane) and $H_3O^+$ (hydronium) were created during the passivation process. The distribution of these bonds/particles were summed based on the bond lengths in Fig. 2 and plotted in Fig. 3 (b). We can see the passivated silicon surface is a mixture of Si–O–Si, Si–O–H, Si–H, Si–$H_2$ and $H_2O$–Si bonds, which is consistent with experimental findings [47–49]. The numbers of these bonds show that silicon surface is dominated by H-termination (Si–H or Si–$H_2$ bonds), which is responsible for the surface hydrophobicity observed in experiment [50]. Si–O–Si bonds exist throughout the oxide film and determine the oxide depth. In addition, the surface passivation process created a large amount of $H_3O^+$, which together with remain $H_2O$ form the resultant water layer.

Fig. 3 (b) shows the distribution of atomic charge H, O and Si atoms in passivation result. O and Si atoms in the oxide film occupy different amounts of charge in comparison to these in water and silicon substrates. In the water film and silicon, O and Si atoms show −0.77 and 0 e, respectively. However, oxidised silicon shows positive charge, the maximum value appears at 1.1 e at the silicon-water interface. This indicates the charge transfer between O and Si atoms during the creation of oxide layer, providing further evidence for the occurrence of an oxidation process. In addition, O atoms in the oxide film have less charge than that in water, ranging from −0.71 to −0.42 e, which is due to the different polarities in Si–O and H–O bonds.

### 3.2. Bias-induced oxidation

The ReaxFF simulation result at 2000 ps is shown in Fig. 5 (a). Apparently, more O atoms penetrated the silicon surface, resulting in an increased oxide thickness. Similarly, the RDF of oxide film is plotted in Fig. 4 and the bonds/particles distribution in oxide film is plotted in Fig. 5 (b). Through the comparison with passivation results in Fig. 2 and Fig. 3 (b), we can see good similarities in both RDF of oxide film and bonds/particles distribution at the oxidised silicon surface. These demonstrate the application of electric field did not apparently modify the chemical structures within oxide film and surface composition,

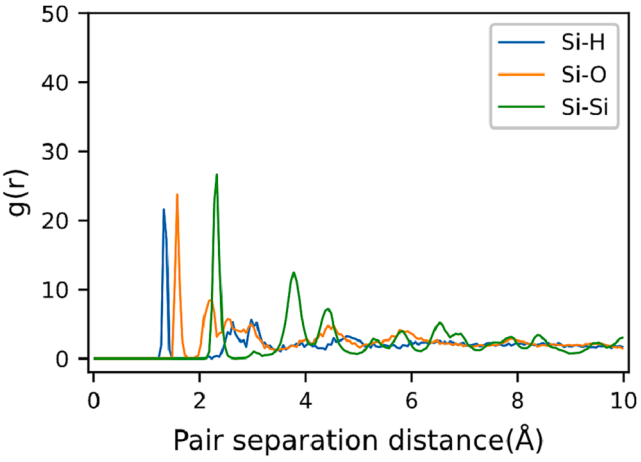


**Fig. 4.** RDF curves for Si–H, Si–O and Si–Si in oxide film formed by bias-induced oxidation.

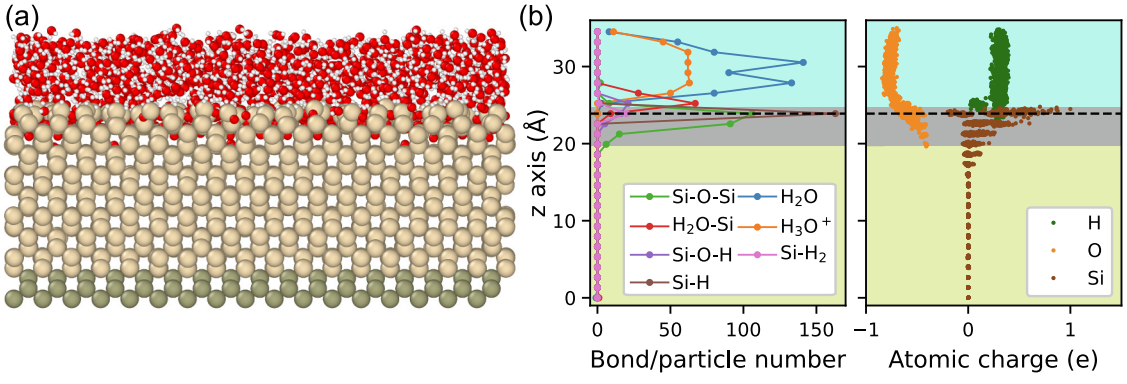


**Fig. 3.** Simulation results for surface passivation. (a) Side view. (b) Distribution of bond/particle numbers and atomic charges along *z* axis, in which shaded regions coloured with wheat, grey and cyan represent silicon, oxide layer and water, respectively. The horizontal dashed line indicates the first atom layer in the initial model. (For interpretation of the references to colour in this figure legend, the reader is referred to the web version of this article.)

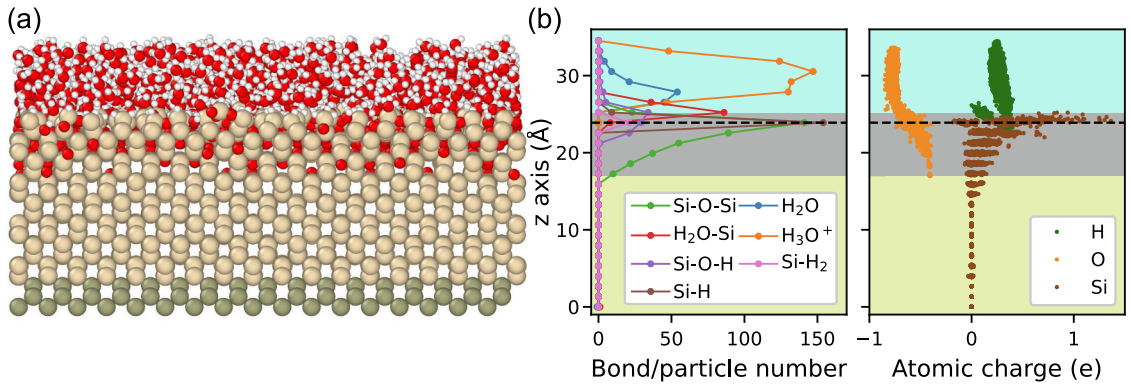


**Fig. 5.** Bias-induced oxidation result. (a) Side view. (b) Distribution of bond/particle numbers and atomic charges along *z* axis, in which shaded regions coloured with wheat, grey and cyan represent silicon, oxide layer and water, respectively. The horizontal dashed line represents the first atomic layer in the initial model. (For interpretation of the references to colour in this figure legend, the reader is referred to the web version of this article.)

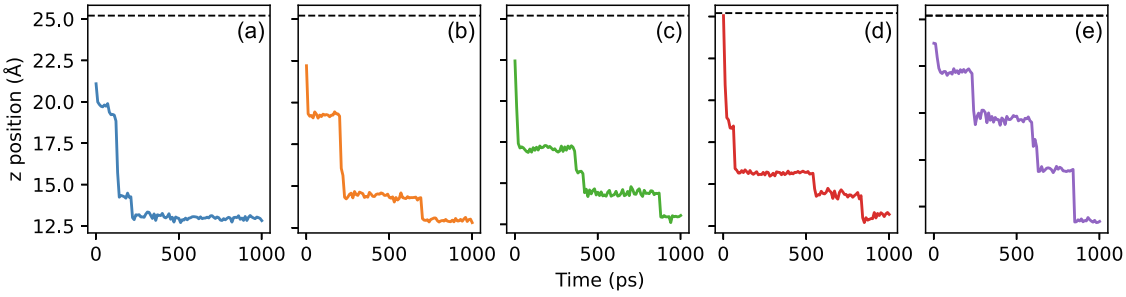


**Fig. 6.** Time evolution of oxide thickness and bond/particle number during the reaction between silicon (100) substrate and 10 Å thick layer of water.

while led to the generation of more Si–O–Si bonds under the oxide surface and increased the oxide thickness. Additionally, Si–O–Si bonds are found to be mostly concentrated near the surface and their number gradually decreases layer by layer throughout the oxide film. The atomic charge distribution in Fig. 5 (b) shows that the application of electric field increased the degree of oxidation on silicon substrate, evidenced by more electropositive Si atoms in the results. Despite the increased O atoms near the surface, a number of Si atoms within the oxide layer remain unoxidized, as indicated by the Si atoms with nearly 0 charge in Fig. 5 (b). This clearly indicates a mixture of Si and $SiO_2$ within the oxide film. Overall, the oxide film is found with a complex chemical structure consisting of amorphous $SiO_2$, adsorbed water, silicon and silicon hydrates, which is consistent with previous simulations and experimental results [12,51].

### 3.3. Reaction process

To reveal the in-process details during surface passivation and bias-induced oxidation, the evolution of the number of bonds/particles and oxide thickness is depicted in Fig. 6, which were counted based on dump files created every 10 ps. In passivation stage, water was consumed and turned into oxide, represented by reduced number of $H_2O$ and increased numbers of Si–O–H and Si–O–Si bonds. In addition, hydrogen atoms from water decomposition either attached to surface silicon atoms and form Si–H/Si–$H_2$ bonds or combined with water molecules and form $H_3O^+$. The evolution curves show that water reacted with silicon rapidly at the beginning of the simulation. A majority of Si–O–H, Si–H, Si–$H_2$ and $H_2O$–Si were created in the first 40 ps and maintained at almost constant amounts in the following reaction up to 1000 ps. From 40 to 1000 ps, the oxide thickness increased from 4 to 5.1 Å. Simultaneously, there was a gradual consumption of $H_2O$, leading to the formation of more Si–O–Si bonds and $H_3O^+$, but at a relatively slow rate.

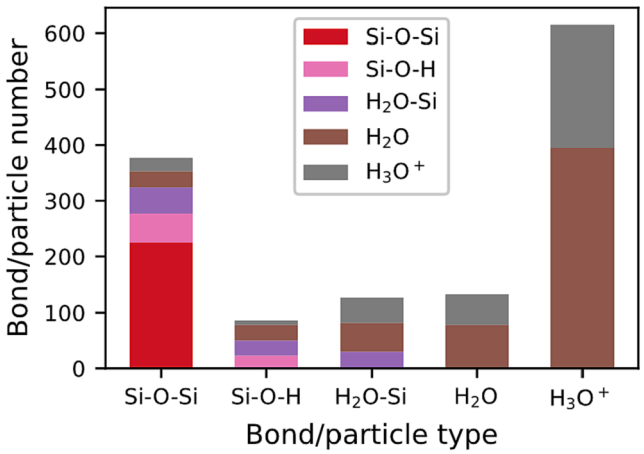


**Fig. 7.** Bar chart showing the bond/particle number of Si–O–Si, Si–O–H, $H_2O$–Si, $H_2O$ and $H_3O^+$ of simulation result at 2000 ps. The bars are colour-coded to represent O atoms in each bond/particle type at 1000 ps.

In bias-induced oxidation stage, an electric field of 3.5 V/nm was applied during 1000–2000 ps. The evolution curves in Fig. 6 show the amounts of Si–O–H, Si–H, Si–$H_2$ and $H_2O$–Si have not changed significantly, which further demonstrates that the action of electric field did not apparently modify the surface composition. However, from 1000 to 2000 ps, the oxide thickness increased from 5.1 to 8.2 Å, the number of $H_2O$ decreased by 472, and the numbers of Si–O–Si and $H_3O^+$ increased by 149 and 282. The number changes of $H_2O$, Si–O–Si and $H_3O^+$ roughly follow 3: 1: 2. Since the numbers of other bonds/particles do not vary

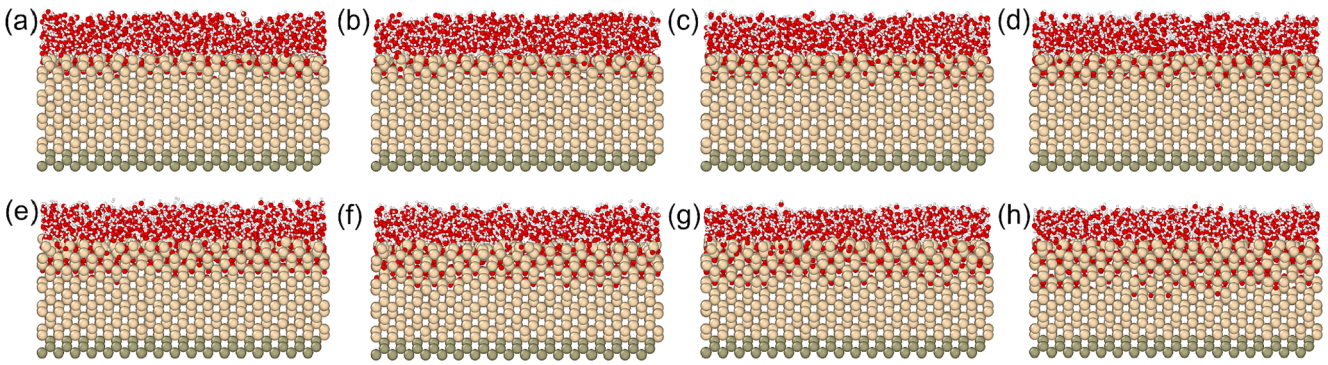


**Fig. 8.** Sides views of simulation results with the application of electric fields with strength ranging from 0 to 7 V/nm.

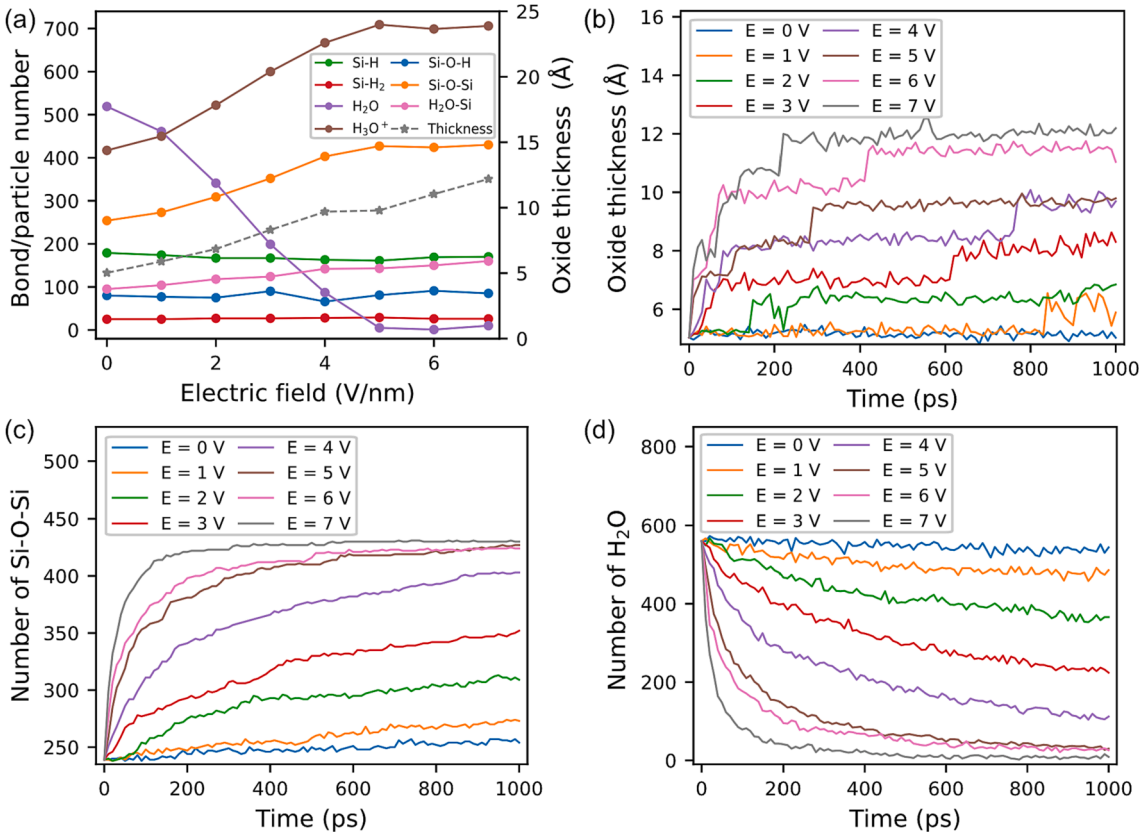


**Fig. 9.** (a) The number of particles/bonds and oxide thickness of simulation results at different electric fields. Evolution of (b) oxide thickness and the number of (c) Si–O–Si bonds and (d) $H_2O$ at electric fields with strength ranging from 0 to 7 V/nm.

significantly during the simulation, this suggests the bias-induced oxidation mainly induces the following reaction:

$$(Si-Si)+3H_2O \xrightarrow{bias} (Si-O-Si)^{2-}+2H_3O^{+} \quad (1)$$

To uncover the reaction process, we tracked all the O atoms in Si–O–Si, Si–O–H, $H_2O$–Si and $H_2O/H_3O^+$ at 2000 ps and summarised the bonds/particles they belong to at 1000 ps, the results of which are shown in Fig. 7. O atoms in Si–O–Si may come from all the bonds/particles that have O atoms. The number of Si–O–Si bonds at 1000 ps (see Fig. 6) indicates all the O atoms in Si–O–Si bonds at 1000 ps remains within the Si–O–Si bonds in the bias-induced oxidation process. In addition, O atoms in Si–O–H only come from Si–O–H, $H_2O$–Si and $H_2O/H_3O^+$; and O atoms in $H_2O$–Si only come from $H_2O$–Si and $H_2O/H_3O^+$. On the basis of above findings, it appears that Si–O–H and $H_2O$–Si act as intermediate products at the surface during the bias-induced oxidation. Specifically, three reactions during the bias-induced oxidation were demonstrated. First, $H_2O$ adsorbs to the silicon surface, forming an $H_2O$–Si bond. Next, the $H_2O$–Si bond dissolves into Si–O–H bond. Then, Si–O–H reacts with one of the surrounding Si atoms to form a Si–O–Si bond. However, we did not observe any O atoms moving from Si–O–Si to Si–O–H and then to $H_2O$–Si, indicating that the reaction cannot proceed in the reverse direction.

## 4. Parametric study

### 4.1. Effect of the electric field

The dependence of different electric fields on bias-induced oxidation was examined through eight groups of simulations. Each group utilised the same initial model with a passivated layer depicted in Fig. 3 (a) but applied different electric fields with varying strengths ranging from 0 to

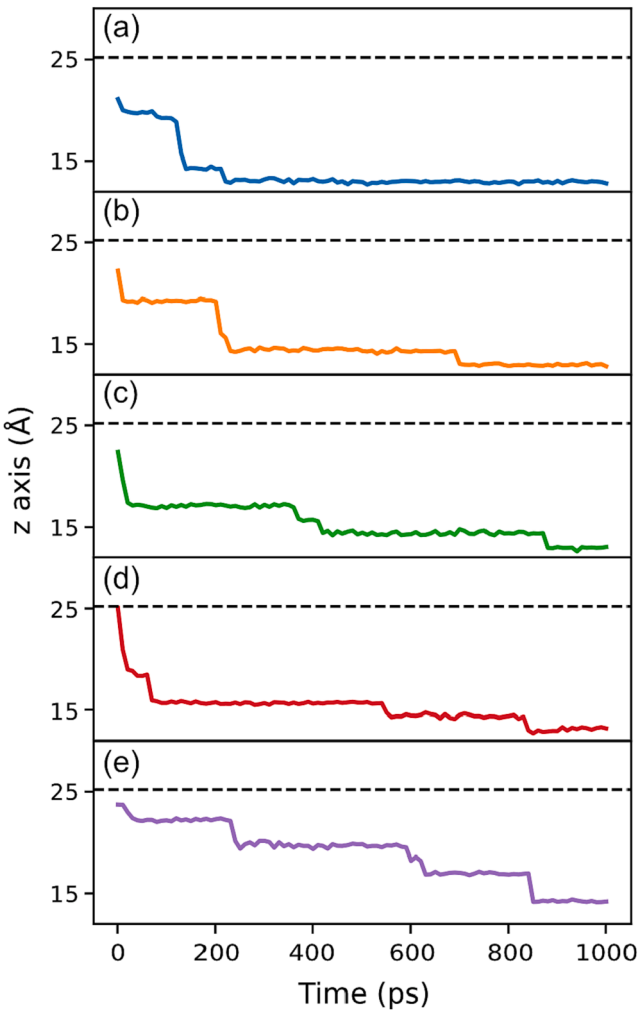


**Fig. 10.** The evolution of *z* positions of bottom five O atoms (a–e) in the oxide layer in Fig. 8 (h). The horizontal dashed line represents the first atom layer in the initial model.

7 V/nm. Group 1 did not apply an electric field to demonstrate the effect of ongoing surface passivation. After simulating the bias-induced oxidation for 1000 ps, the results in all groups are shown in Fig. 8. These results indicate a noticeable increase in the penetration of O atoms into the silicon substrate as the electric field strength increases.

Fig. 9 (a) illustrates the number of bonds/particles and oxide thickness in simulation results to determine the influence of different electric fields on the chemical composition. The numbers of surface bonds including Si–O–H, $H_2O$–Si, Si–H and Si–$H_2$ are not drastically affected by different electric fields; while the consumption of $H_2O$ and the creation of Si–O–Si and $H_3O^+$ are enhanced as electric field increases from 0 to 5 V/nm. The number changes of $H_2O$, Si–O–Si and $H_3O^+$ during each simulation group also approximately follow 3: 1: 2. This further demonstrates the reaction (1) dominates the bias-induced oxidation.

The evolution curves depicted in Fig. 9 (c) and (d) suggest that the rate of reaction (1) increases with increased electric field strength, as the enhanced electric field clearly accelerates the production rate of Si–O–Si bonds and consumption rate of $H_2O$, particularly in the first 100 ps. In addition, the reaction rate was found to be correlated with the amount of $H_2O$ in the water layer, as indicated by the reduced generation rate of Si–O–Si with a decrease in the amount of $H_2O$ remaining in the water layer. According to the simulation results shown in Fig. 9 (a), the numbers of Si–O–Si bonds in simulation results reached approximately 430 at electric fields higher than 5 V/nm and did not increase further. This indicates that the reaction ceased when the $H_2O$ in reaction system was depleted. In the actual LAO experiments, water depletion should be more difficult to occur than in the simulation with limited length scales. This is due to the presence of the water layer on both the tool and substrate surfaces in the atmospheric humidity, which allows for the continuous diffusion of water molecules to replenish any depletion during the LAO process. As a result, the oxidation can continue, with its reaction rate and duration determined by the diffusion rate of water [52].

Fig. 9 (a) indicates that the oxide thickness of the simulation results increases in a linear-like fashion with respect to the electric field strength and Fig. 9 (b) demonstrates that the oxide thickness increases layer by layer during the progression in each group of simulation. Both findings are consistent with results in previous experimental and simulation research [31,53,54]. As the strength of electric field exceeds 5 V/nm, the oxide thickness increases by one layer of silicon atoms even in the absence of an increase in the number of Si–O–Si bonds. Fig. 10 depicts the evolution of *z* positions of selected O atoms in Fig. 8 (h). Between 300 and 1000 ps, no additional Si–O–Si bonds were created (as shown in Fig. 9 (c)), but the existing negatively charged O atoms in Si–O–Si were found to diffuse into the silicon substrate in response to the electric field. This indicates that electric field induced directional movement of O atoms can contribute to the oxidation growth, which, together with reaction (1) constitutes the oxidation growth mechanism in bias-induced oxidation process.

### 4.2. *Effect of the humidity*

As different humidity levels lead to different adsorbed water layer thicknesses, the dependence of humidity on bias-induced oxidation can be examined by simulating the models shown in Fig. 1 (a–d). Similar to the simulation settings in Section 3, electric field was only applied from 1000 to 2000 ps. Fig. 11 shows the simulation results at 2000 ps, which shows the increasing penetration of O atoms into the silicon substrate as humidity increases.

Fig. 12 (a) and (b) plot the bonds/particles number and oxide thickness of surface passivation and bias-induced oxidation results at the different humidity levels. The number of bonds that only exist at the surface does not appear to be affected by water layer thicknesses in both passivation and bias-induced oxidation results. However, the numbers of Si–O–Si bonds in both simulation results increase with an increasing water layer thickness, and the increase is more pronounced in the bias-induced oxidation results. As the water layer thickness increases from 7 to 17 Å (relative humidity approximately from 20% to 90%), the number of Si–O–Si bonds increases from 287 to 665 and the oxide thickness increases from 8.24 to 12.27 Å. These results show that a higher humidity can enhance the degree of oxidation for bias-induced oxidation

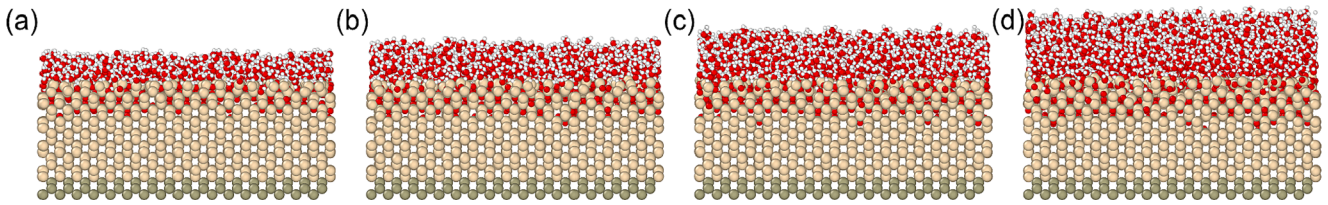


**Fig. 11.** Sides views of simulation results of bias-induced oxidation on passivated silicon surface at the humidity levels of 20%, 40%, 70% and 90%.

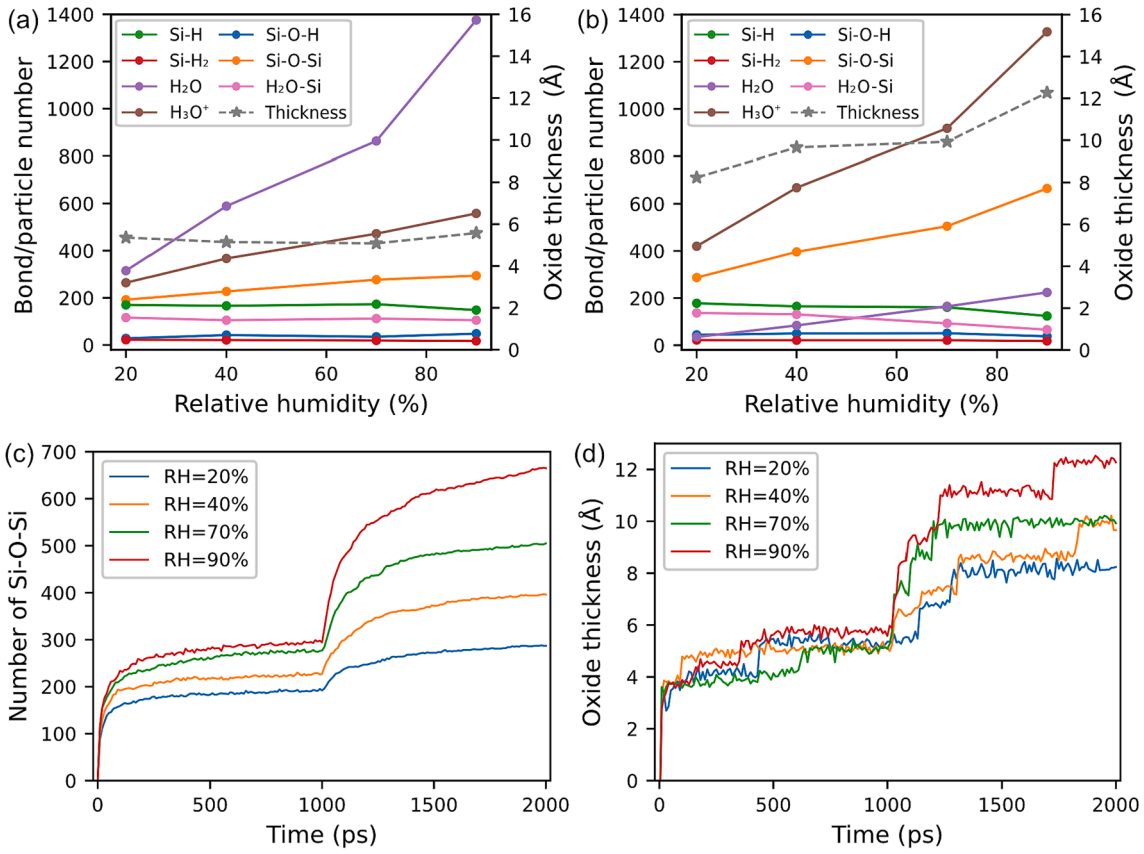


**Fig. 12.** The number of bonds/particles and oxide thickness of (a) passivation results and (b) bias-induced oxidation results at different humidity levels. Time evolution of (c) the number of Si–O–Si bonds and (d) oxide thickness during passivation and bias-induced oxidation at different humidity levels.

process, which aligns with and may provide a reaction-based interpretation of experimental observations [55]. Fig. 12 (c) and (d) show the evolution of the number of Si–O–Si bonds and oxide thickness, which apparently display an enhanced oxidation rate at increased water layer thicknesses. The influencing mechanism should then be related to the increased number of $H_2O$ within the water layer, which facilitates the happening of reaction (1).

## 5. Conclusions

In the paper, ReaxFF MD simulations were performed to study the initial passivation and subsequent bias-induced oxidation on Si (100) surface, in order to gain an atomistic insight into the reaction mechanism of the LAO process. During the bias-induced oxidation, the application of an electric field facilitates a series of reactions, where O atoms can move from water layer ($H_2O/H_3O^+$) to oxide surface ($H_2O$–Si and Si–O–H), and then deep in the oxide film (Si–O–Si). The numbers of intermediate products ($H_2O$–Si and Si–O–H), Si–H and Si–$H_2$ bonds on the surface were not apparently altered during the bias-induced oxidation. Overall, the bias-induced oxidation mainly consumed $H_2O$ within the water layer and resulted in the formation of Si–O–Si bonds beneath the oxide surface. The parametric study further demonstrated that the main reaction in bias-induced oxidation can be notably enhanced with the increase of the strength of the electric field and the amount of $H_2O$ in water layer. These results provide an atomistic understanding on the physical–chemical reaction mechanism in LAO, which is useful to develop novel process-control strategy to enable the patterning at the sub-10 nm scale and even atomic scale.

## CRediT authorship contribution statement

**Jian Gao:** Conceptualization, Methodology, Software, Formal analysis, Data curation, Investigation, Writing – original draft, Writing – review & editing, Visualization. **Xichun Luo:** Funding acquisition, Project administration, Resources, Supervision, Writing – review & editing. **Wenkun Xie:** Funding acquisition, Investigation, Writing – review & editing. **Yi Qin:** Supervision. **Rashed Md. Murad Hasan:** Resources, Methodology, Software. **Pengfei Fan:** Software.

## Declaration of Competing Interest

The authors declare that they have no known competing financial interests or personal relationships that could have appeared to influence the work reported in this paper.

## Data availability

All data underpinning this publication are openly available from the University of Strathclyde Knowledge Base at https://doi.org/10.15129/773fb2bc-7a7e-49de-96e5-04b55251f2db.

*Acknowledgements*

Results were obtained using the ARCHIE-WeSt High Performance Computer (www.archie-west.ac.uk) based at the University of Strathclyde. The authors would like to thank EPSRC (EP/K018345/1, EP/T024844/1, EP/V055208/1) and UKRI Fellowship programme (EP/X021963/1) to provide financial support to this research.

*Data statement*

All data underpinning this publication are openly available from the University of Strathclyde Knowledge Base at https://doi.org/10.15129/773fb2bc-7a7e-49de-96e5-04b55251f2db.

## References


[1] Y.K. Ryu, R. Garcia, Advanced oxidation scanning probe lithography, Nanotechnology. 28 (2017), 142003, https://doi.org/10.1088/1361-6528/aa5651.

[2] C. Ovenden, I. Farrer, M.S. Skolnick, J. Heffernan, Nanoscale wafer patterning using SPM induced local anodic oxidation in InP substrates, Semicond. Sci. Technol. 37 (2022), 025001, https://doi.org/10.1088/1361-6641/ac3f20.

[3] M. Pea, M. De Seta, L. Di Gaspare, L. Persichetti, A.M. Scaparro, V. Miseikis, C. Coletti, A. Notargiacomo, Submicron Size Schottky Junctions on As-Grown Monolayer Epitaxial Graphene on Ge(100): A Low-Invasive Scanned-Probe-Based Study, ACS Appl. Mater. Interfaces. 11 (2019) 35079–35087, https://doi.org/10.1021/acsami.9b09681.

[4] C.-F. Chen, S.-D. Tzeng, H.-Y. Chen, S. Gwo, Silicon microlens structures fabricated by scanning-probe gray-scale oxidation, Opt. Lett. 30 (2005) 652, https://doi.org/10.1364/OL.30.000652.

[5] R.M.M. Hasan, X.C. Luo, J.N. Sun, Rolling Nanoelectrode Lithography, Micromachines. 11 (2020) 656, https://doi.org/10.3390/mi11070656.

[6] J. Gao, X.C. Luo, F.Z. Fang, J.N. Sun, Fundamentals of atomic and close-to-atomic scale manufacturing: A review, Int. J. Extreme Manuf. 4 (2021), 012001, https://doi.org/10.1088/2631-7990/ac3bb2.

[7] B. Theogene, J. Cui, X. Wang, W. Wang, X. Mei, P. Yi, X. Yang, X. He, H. Xie, 3-D finite element calculation of electric field enhancement for nanostructures fabrication mechanism on silicon surface with AFM tip induced local anodic oxidation, Integr. Ferroelectr. 190 (2018) 129–141, https://doi.org/10.1080/10584587.2018.1457346.

[8] T. Cramer, F. Zerbetto, R. García, Molecular Mechanism of Water Bridge Buildup: Field-Induced Formation of Nanoscale Menisci, Langmuir. 24 (2008) 6116–6120, https://doi.org/10.1021/la800220r.

[9] H.J. Choi, J.Y. Kim, S.D. Hong, M.Y. Ha, J. Jang, Molecular simulation of the nanoscale water confined between an atomic force microscope tip and a surface, Mol. Simul. 35 (2009) 466–472, https://doi.org/10.1080/08927020802635129.

[10] J. Gao, X.C. Luo, W. Chang, Z. Wang, Y. Yan, Y. Geng, Insight into Atomic-Scale Adhesion at the C-Cu Interface During the Initial Stage of Nanoindentation, Nanomanufacturing Metrol. 5 (2022) 250–258, https://doi.org/10.1007/s41871-022-00149-3.

[11] X.C. Luo, X.G. Guo, J. Gao, S. Goel, S.Z. Chavoshi, Molecular Dynamics Simulation of Advanced Machining Processes, in: Adv. Mach. Sci., CRC Press, 2022: pp. 385–424. https://doi.org/10.1201/9780429160011-14.

[12] J. Wen, T. Ma, W. Zhang, A.C.T. van Duin, X. Lu, Surface Orientation and Temperature Effects on the Interaction of Silicon with Water: Molecular Dynamics Simulations Using ReaxFF Reactive Force Field, J. Phys. Chem. A. 121 (2017) 587–594, https://doi.org/10.1021/acs.jpca.6b11310.

[13] Y. Sun, Y. Liu, X. Chen, Z. Zhai, F. Xu, Y. Liu, Micromechanism of oxygen transport during initial stage oxidation in Si(100) surface: A ReaxFF molecular dynamics simulation study, Appl. Surf. Sci. 406 (2017) 178–185, https://doi.org/10.1016/j.apsusc.2017.01.302.

[14] S. Yuan, X. Wang, H. Zhang, S. Yuan, Reactive Molecular Dynamics on the Oxidation of H-Si(100) Surface: Effect of Humidity and Temperature, J. Phys. Chem. C. 124 (2020) 1932–1940, https://doi.org/10.1021/acs.jpcc.9b08702.

[15] Y. Sun, Y.-L. Liu, S. Izumi, X.-F. Chen, Z. Zhai, S.-H. Tian, Initial stage oxidation on nano-trenched Si(1 0 0) surface, J. Phys. Appl. Phys. 51 (2018), 015305, https://doi.org/10.1088/1361-6463/aa99ab.

[16] O. Assowe, O. Politano, V. Vignal, P. Arnoux, B. Diawara, O. Verners, A.C.T. van Duin, Reactive molecular dynamics of the initial oxidation stages of Ni(111) in pure water: effect of an applied electric field, J. Phys. Chem. A. 116 (2012) 11796–11805, https://doi.org/10.1021/jp306932a.

[17] L. Ai, H. Huang, Y. Zhou, M. Chen, Y. Lü, The oxidation of Fe/Ni alloy surface with supercritical water: A ReaxFF molecular dynamics simulation, Appl. Surf. Sci. 553 (2021), 149519, https://doi.org/10.1016/j.apsusc.2021.149519.

[18] J. Yeon, S.C. Chowdhury, J.W. Gillespie Jr., Hydroxylation and water-surface interaction for S-glass and silica glass using ReaxFF based molecular dynamics simulations, Appl. Surf. Sci. 608 (2023), 155078, https://doi.org/10.1016/j.apsusc.2022.155078.

[19] X. Jiang, Y. Hu, L. Ling, X. Wang, The initial wet oxidation process on Fe-Cr alloy surface: Insights from ReaxFF molecular dynamic simulations, Appl. Surf. Sci. 548 (2021), 149159, https://doi.org/10.1016/j.apsusc.2021.149159.

[20] L. Ai, Y. Zhou, H. Huang, Y. Lv, M. Chen, A reactive force field molecular dynamics simulation of nickel oxidation in supercritical water, J. Supercrit. Fluids. 133 (2018) 421–428, https://doi.org/10.1016/j.supflu.2017.10.025.

[21] J. Wen, T. Ma, W. Zhang, G. Psofogiannakis, A.C.T. van Duin, L. Chen, L. Qian, Y. Hu, X. Lu, Atomic insight into tribochemical wear mechanism of silicon at the Si/SiO2 interface in aqueous environment: Molecular dynamics simulations using ReaxFF reactive force field, Appl. Surf. Sci. 390 (2016) 216–223, https://doi.org/10.1016/j.apsusc.2016.08.082.

[22] M. Wang, F. Duan, Atomic-Level Material Removal Mechanisms of Si(110) Chemical Mechanical Polishing: Insights from ReaxFF Reactive Molecular Dynamics Simulations, Langmuir. 37 (2021) 2161–2169, https://doi.org/10.1021/acs.langmuir.0c03416.

[23] S. Yuan, X. Guo, P. Li, S. Zhang, M. Li, Z. Jin, R. Kang, D. Guo, F. Liu, L. Zhang, Atomistic understanding of interfacial processing mechanism of silicon in water environment: A ReaxFF molecular dynamics simulation, Front, Mech. Eng. 16 (2021) 570–579, https://doi.org/10.1007/s11465-021-0642-6.

[24] S. Yuan, X. Guo, S. Zhang, C. Zhang, P. Li, Z. Jin, R. Kang, D. Guo, Influence mechanism of defects on the subsurface damage and structural evolution of diamond in CMP process, Appl. Surf. Sci. 566 (2021), 150638, https://doi.org/10.1016/j.apsusc.2021.150638.

[25] Z. Shi, Z. Jin, X. Guo, S. Yuan, J. Guo, Insights into the atomistic behavior in diamond chemical mechanical polishing with OH environment using ReaxFF molecular dynamics simulation, Comput. Mater. Sci. 166 (2019) 136–142, https://doi.org/10.1016/j.commatsci.2019.05.001.

[26] X. Guo, X. Wang, Z. Jin, R. Kang, Atomistic mechanisms of Cu CMP in aqueous H2O2: Molecular dynamics simulations using ReaxFF reactive force field, Comput. Mater. Sci. 155 (2018) 476–482, https://doi.org/10.1016/j.commatsci.2018.09.022.

[27] J. Yeon, A.C.T. van Duin, S.H. Kim, Effects of Water on Tribochemical Wear of Silicon Oxide Interface: Molecular Dynamics (MD) Study with Reactive Force Field (ReaxFF), Langmuir. 32 (2016) 1018–1026, https://doi.org/10.1021/acs.langmuir.5b04062.

[28] Y. Wang, J. Qin, J. Xu, J. Sun, L. Chen, L. Qian, M. Kubo, Definition of Atomic-Scale Contact: What Dominates the Atomic-Scale Friction Behaviors? Langmuir. 38 (2022) 11699–11706, https://doi.org/10.1021/acs.langmuir.2c01786.

[29] F. Tavazza, T.P. Senftle, C. Zou, C.A. Becker, A.C.T. van Duin, Molecular Dynamics Investigation of the Effects of Tip-Substrate Interactions during Nanoindentation, J. Phys. Chem. C. 119 (2015) 13580–13589, https://doi.org/10.1021/acs.jpcc.5b01275.

[30] R.M.M. Hasan, O. Politano, X.C. Luo, ReaxFF molecular dynamics simulation study of nanoelectrode lithography oxidation process on silicon (100) surface, Appl. Surf. Sci. 496 (2019), 143679, https://doi.org/10.1016/j.apsusc.2019.143679.

[31] R.M.M. Hasan, O. Politano, X.C. Luo, Substrate orientation effects on nanoelectrode lithography: ReaxFF molecular dynamics and experimental study, J. Phys. Appl. Phys. 53 (2020), 295108, https://doi.org/10.1088/1361-6463/ab86e2.

[32] S. Plimpton, Fast Parallel Algorithms for Short-Range Molecular Dynamics, J. Comput. Phys. 117 (1995) 1–19, https://doi.org/10.1006/jcph.1995.1039.

[33] J. Wen, T. Ma, W. Zhang, A.C.T. van Duin, X. Lu, Atomistic mechanisms of Si chemical mechanical polishing in aqueous H2O2: ReaxFF reactive molecular dynamics simulations, Comput. Mater. Sci. 131 (2017) 230–238, https://doi.org/10.1016/j.commatsci.2017.02.005.

[34] H.M. Aktulga, J.C. Fogarty, S.A. Pandit, A.Y. Grama, Parallel reactive molecular dynamics: Numerical methods and algorithmic techniques, Parallel Comput. 38 (2012) 245–259, https://doi.org/10.1016/j.parco.2011.08.005.

[35] T. Hattori, Y. Ejiri, K. Saito, M. Yasutake, Fabrication of nanometer-scale structures using atomic force microscope with conducting probe, J. Vac. Sci. Technol. Vac. Surf. Films. 12 (1994) 2586–2590, https://doi.org/10.1116/1.579062.

[36] P. Avouris, T. Hertel, R. Martel, Atomic force microscope tip-induced local oxidation of silicon: kinetics, mechanism, and nanofabrication, Appl. Phys. Lett. 71 (1997) 285–287, https://doi.org/10.1063/1.119521.

[37] D.B. Asay, S.H. Kim, Evolution of the Adsorbed Water Layer Structure on Silicon Oxide at Room Temperature, J. Phys. Chem. B. 109 (2005) 16760–16763, https://doi.org/10.1021/jp053042o.

[38] L. Martínez, R. Andrade, E.G. Birgin, J.M. Martínez, PACKMOL: A package for building initial configurations for molecular dynamics simulations, J. Comput. Chem. 30 (2009) 2157–2164, https://doi.org/10.1002/jcc.21224.

[39] K. Chenoweth, A.C.T. van Duin, W.A. Goddard, ReaxFF Reactive Force Field for Molecular Dynamics Simulations of Hydrocarbon Oxidation, J. Phys. Chem. A. 112 (2008) 1040–1053, https://doi.org/10.1021/jp709896w.

[40] M.R. Weismiller, A.C.T. van Duin, J. Lee, R.A. Yetter, ReaxFF Reactive Force Field Development and Applications for Molecular Dynamics Simulations of Ammonia Borane Dehydrogenation and Combustion, J. Phys. Chem. A. 114 (2010) 5485–5492, https://doi.org/10.1021/jp100136c.

[41] A. Stukowski, Visualization and analysis of atomistic simulation data with OVITO–the Open Visualization Tool, Model. Simul. Mater. Sci. Eng. 18 (2009), 015012, https://doi.org/10.1088/0965-0393/18/1/015012.

[42] L. Pauling, The nature of the chemical bond, Cornell University Press, Ithaca N. Y. (1960).

[43] W.D. Luedtke, U. Landman, Preparation and melting of amorphous silicon by molecular-dynamics simulations, Phys. Rev. B. 37 (1988) 4656–4663, https://doi.org/10.1103/PhysRevB.37.4656.

[44] R.J. Bell, P. Dean, The structure of vitreous silica: Validity of the random network theory, Philos. Mag. 25 (1972) 1381–1398, https://doi.org/10.1080/14786437208223861.

[45] D.I. Grimley, A.C. Wright, R.N. Sinclair, Neutron scattering from vitreous silica IV. Time-of-flight diffraction, J. Non Cryst. Solids. 119 (1990) 49–64.

[46] M.V. Coleman, D.J.D. Thomas, The structure of silicon oxide films, Phys. Status Solidi B. 22 (1967) 593–602, https://doi.org/10.1002/pssb.19670220231.

[47] M. Chander, Y.Z. Li, J.C. Patrin, J.H. Weaver, Si(100)-(2×1) surface defects and dissociative and nondissociative adsorption of H 2 O studied with scanning tunneling microscopy, Phys. Rev. B. 48 (1993) 2493–2499, https://doi.org/10.1103/PhysRevB.48.2493.

[48] M.K. Weldon, B.B. Stefanov, K. Raghavachari, Y.J. Chabal, Initial H 2 O -induced Oxidation of Si(100)– (2 × 1), Phys. Rev. Lett. 79 (1997) 2851–2854, https://doi.org/10.1103/PhysRevLett.79.2851.

[49] G.J. Pietsch, Y.J. Chabal, G.S. Higashi, Infrared-absorption spectroscopy of Si(100) and Si(111) surfaces after chemomechanical polishing, J. Appl. Phys. 78 (1995) 1650–1658, https://doi.org/10.1063/1.360721.
[50] G.J. Pietsch, Y.J. Chabal, G.S. Higashi, The atomic-scale removal mechanism during chemo-mechanical polishing of Si(100) and Si(111), Surf. Sci. 331–333 (1995) 395–401, https://doi.org/10.1016/0039-6028(95)00292-8.
[51] J.A. Dagata, T. Inoue, J. Itoh, H. Yokoyama, Understanding scanned probe oxidation of silicon, Appl. Phys. Lett. 73 (1998) 271–273, https://doi.org/10.1063/1.121777.
[52] E.S. Snow, G.G. Jernigan, P.M. Campbell, The kinetics and mechanism of scanned probe oxidation of Si, Appl. Phys. Lett. 76 (2000) 1782–1784, https://doi.org/10.1063/1.126166.
[53] A.S. Kozhukhov, D.V. Scheglov, L.I. Fedina, A.V. Latyshev, The initial stages of atomic force microscope based local anodic oxidation of silicon, AIP Adv. 8 (2018), 025113, https://doi.org/10.1063/1.5007914.
[54] M. Calleja, R. García, Nano-oxidation of silicon surfaces by noncontact atomic-force microscopy: Size dependence on voltage and pulse duration, Appl. Phys. Lett. 76 (2000) 3427–3429. 10.1063/1.126856.
[55] M.S. Johannes, D.G. Cole, R.L. Clark, Three-dimensional design and replication of silicon oxide nanostructures using an atomic force microscope, Nanotechnology. 18 (2007), 345304, https://doi.org/10.1088/0957-4484/18/34/345304.